Shear-Induced Anisotropy in Rough Elastomer Contact

R. Sahli,[1] G. Pallares,[1,2] A. Papangelo,[3,4] M. Ciavarella,[3,4] C. Ducottet,[5] N. Ponthus,[1] and J. Scheibert[1,*]
[1]Univ Lyon, Ecole Centrale de Lyon, ENISE, ENTPE, CNRS, Laboratoire de Tribologie et Dynamique des Systèmes LTDS, UMR 5513, F-69134 Ecully, France
[2]CESI, LINEACT, Zone Aéroportuaire Méditerranée, 34130 Mauguio, France
[3]Dipartimento di Meccanica, Matematica e Management, Politecnico di Bari, Viale Japigia 182, 70126 Bari, Italy
[4]Hamburg University of Technology, Department of Mechanical Engineering, Am Schwarzenberg-Campus 1, 21073 Hamburg, Germany
[5]Univ Lyon, UJM-Saint-Etienne, CNRS, IOGS, Laboratoire Hubert Curien UMR5516, F-42023 Saint-Etienne, France

(Received 6 March 2019; published 30 May 2019)

True contact between randomly rough solids consists of myriad individual microjunctions. While their total area controls the adhesive friction force of the interface, other macroscopic features, including viscoelastic friction, wear, stiffness, and electric resistance, also strongly depend on the size and shape of individual microjunctions. We show that, in rough elastomer contacts, the shape of microjunctions significantly varies as a function of the shear force applied to the interface. This process leads to a growth of anisotropy of the overall contact interface, which saturates in the macroscopic sliding regime. We show that smooth sphere-plane contacts have the same shear-induced anisotropic behavior as individual microjunctions, with a common scaling law over 4 orders of magnitude in the initial area. We discuss the physical origin of the observations in light of a fracture-based adhesive contact mechanics model, described in the companion article, which captures the smooth sphere-plane measurements. Our results shed light on a generic, overlooked source of anisotropy in rough elastic contacts, not taken into account in current rough contact mechanics models.

DOI: 10.1103/PhysRevLett.122.214301

Real contact between rough solids occurs only in randomly distributed small regions of the interface (microjunctions) [1,2]. The adhesion component of the friction force is proportional to the total area of all microjunctions [3–8]. In contrast, many other macroscopic contact properties (e.g., electric and heat resistance [9,10], normal and shear stiffnesses [11], wear [12], and viscoelastic friction [13]) also depend on the details of the real contact morphology, including the number, size, spatial distribution, and shape of individual microjunctions. In this context, it is clear that any phenomenon affecting the real contact morphology of an interface will also affect all of its above-mentioned physical properties.

The real contact morphology of rough interfaces depends both on loading (e.g., pressure and contact time [14] and sliding velocity [15]) and system parameters (e.g., adhesion between the solids [16] and the spectral contents of the surface roughness [13,17–19]). One of the important descriptors of morphology is the degree of anisotropy of the interface. Rough contact anisotropy may occur for various reasons: anisotropic roughness [20], anisotropic bulk material behavior, or viscoelasticity in the gross sliding regime [15]. The very same reasons also yield anisotropic contact shapes at the interface between smooth axisymmetric bodies, for instance, in sphere-plane geometry [21–24], thus suggesting common physical origins.

Interestingly, in such smooth sphere-plane contacts, another source of anisotropy has been observed: an initially circular contact becomes less and less axisymmetric as it is increasingly sheared [7,25–29]. It is thus natural to hypothesize that a similar growth of anisotropy may also occur in multicontact interfaces under shear. Such a behavior would imply that many transport, mechanical, or tribological properties of a rough contact are not intrinsic features of the interface but are actually dynamical quantities that evolve with the amount of shear applied. In order to test this hypothesis, we further analyze an extensive series of experiments performed on various elastomeric multicontacts, in which the evolution of the morphology of the real contact is monitored optically as the shear force is increased from pure normal contact to gross sliding. All experimental details can be found in Ref. [7], while the main points are summarized here.

We make centimeter-sized contact [Fig. 1(a)] between a flat, smooth bare glass slider and a flat, rough cross-linked polydimethylsiloxane (PDMS) block (rms roughness 26 μm; see a typical power spectrum density in the Supplemental Material [30]), under constant normal force P in the range 0.98–6.40 N [i.e., a ratio p/E^* in the range 0.0006–0.0043, with p being the average pressure applied, $E^* = E/(1-\nu^2)$, and E and ν being the Young's modulus and Poisson's ratio of the PDMS, respectively]. We

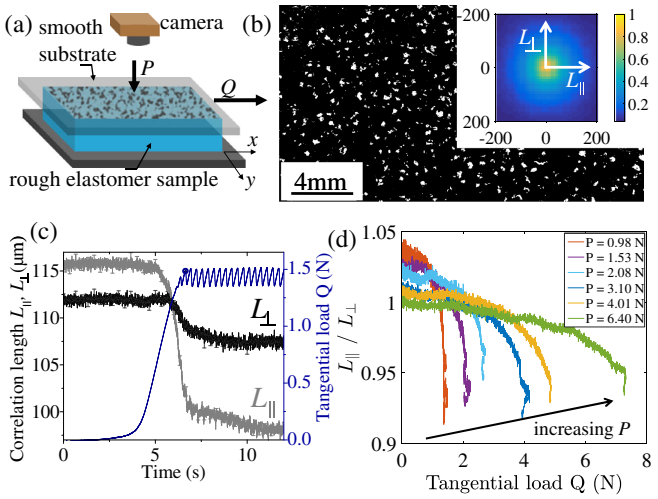

FIG. 1. (a) Sketch of the experimental setup. (b) Typical binarized image of a multicontact. $P = 6.40$ N. (Inset) Normalized autocorrelation function of the image shown in the main panel. The correlation lengths $L_{\parallel}$ and $L_{\perp}$ are obtained through fitting with $e^{-\sqrt{x^2/L_{\parallel}{}^2+y^2/L_{\perp}{}^2}}$ [30]. (c) Concurrent time evolutions of Q, $L_{\parallel}$, and $L_{\perp}$ for the interface of (b). ∘, static friction peak Q_s; error bar, 95% confidence interval. (d) Evolution of $L_{\parallel}/L_{\perp}$ vs Q for various normal forces.

optionally coat the glass surface, either with grafted PDMS chains or with a layer of cross-linked PDMS, to change its adhesive and frictional properties. We drive the slider horizontally towards macrosopic sliding, at constant velocity V in the range 0.05–1 mm/s, while we monitor the tangential force Q. Simultaneously, we image *in situ* the contact and access highly contrasted pictures, which we efficiently binarize using automatic thresholding [30], enabling identification of each microjunction [the white spots in Fig. 1(b)]. In the following, we present data only for PDMS-glass interfaces: PDMS–crosslinked-PDMS interfaces behave similarly, despite a slight initial anisotropy, while PDMS–grafted-PDMS interfaces show negligible evolution under shear due to low frictional strength [7]. Also, we observed only a weak effect of V, so we will show results only for $V = 0.1$ mm/s.

To assess whether the degree of anisotropy of our rough contacts changes under shear, we compute, for each binarized image, its normalized autocorrelation function, a typical example of which is shown in Fig. 1(b) (inset). We then fit this function (see the caption of Fig. 1) to extract two correlation lengths, $L_{\parallel}$ and $L_{\perp}$, in the directions parallel and orthogonal to shear loading, respectively. Figure 1(c) shows a typical concurrent evolution of the correlation lengths and the tangential force Q as the interface is driven from its initial state (pure normal force) to macroscopic sliding. We find that, for $Q = 0$, $L_{\parallel}$ and $L_{\perp}$ are roughly equal (less than a 5% difference) for all normal forces, showing that the contact is initially isotropic. As soon as Q increases, $L_{\parallel}$ is found to significantly decrease, typically by 10%–15%, while $L_{\perp}$ varies much less. Both correlation lengths stabilize after Q has reached the static friction peak value, Q_s, and the interface has entered a macroscopic sliding regime. We quantify contact anisotropy by the ratio $L_{\parallel}/L_{\perp}$, shown as a function of the tangential force Q in Fig. 1(d). We find that $L_{\parallel}/L_{\perp}$ decreases by ∼7%–12%, with larger decays for smaller normal forces. Those results validate our initial hypothesis (rough contacts undergo a growing anisotropy under increasing shear) with, at the onset of sliding, a significantly reduced characteristic length scale of the real contact along the loading direction.

What is the microscopic origin of this growing anisotropy? To answer this question, we track the individual microjunctions along the shearing experiments (tracking performed as in Ref. [7]) and extract the time evolution of their area and shape and the location of their center of mass. For each tracked microjunction i, we define its mean size a_i from its area A_i: $a_i = \sqrt{A_i/\pi}$. We first find that, for all experiments, the values of $L_{\parallel}$ and $L_{\perp}$ match the mean size of individual microjunctions at the interface [Fig. 2(a)]. This suggests that the observed growth of macroscopic anisotropy reflects a change in shape of each individual microjunction, rather than an anisotropic modification of their spatial organisation along the contact plane. Indeed, in the latter case, the characteristic length scales

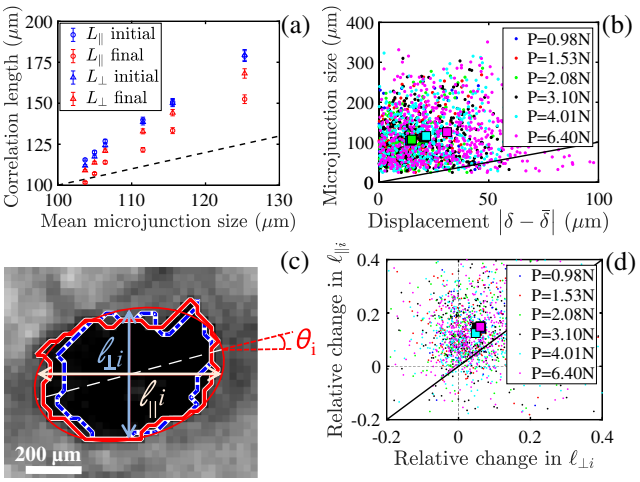

FIG. 2. (a) Macroscopic correlation lengths along the directions parallel (empty circle) and orthogonal (empty triangle) to shear, for $Q = 0$ (blue) and $Q = Q_s$ (red), vs average microjunction size, for various P. Error bar, 95% confidence interval. (b) Filled circle, microjunction size vs norm of its excursion from the initial real contact pattern for the experiments of (a); Square, data barycenter for each P; solid line, equality line. (c) Typical microjunction image. Solid red (dashed blue) line, contour for $Q = 0$ ($Q = Q_s$); red ellipse, equivalent ellipse showing $\ell_{\parallel i}$, $\ell_{\perp i}$, and θ_i. (d) Relative change of $\ell_{\parallel i}$ vs relative change of $\ell_{\perp i}$ for individual microjunctions in the experiments of (a) and (b). Square, data barycenter, as in (b); solid line, equality line.

measured would have been larger, reflecting the size of possible clusters of microjunctions.

To check this hypothesis, we measure $|\delta_i - \bar{\delta}|$, the displacement of microjunction i with respect to the average motion of all microjunctions, $\bar{\delta}$, at the onset of sliding (when $Q = Q_s$). Note that $\bar{\delta}$ varies from about 50 to 150 μm when the normal force is increased from about 1 to 6.4 N. $|\delta_i - \bar{\delta}|$ quantifies how much the initial pattern of microjunctions along the interface has been modified upon shearing. Figure 2(b) represents a_i as a function of $|\delta_i - \bar{\delta}|$ for all tracked microjunctions in all experiments. The large majority of the points are above the equality line, meaning that the microjunctions move with respect to their initial neighborhood by less than their own size. Such an observation indicates that the microjunction pattern forming the real contact is virtually unaffected by shear. Hence, we conclude that the evolution of the correlation length of the real contact does not originate from the relative displacement of microjunctions. This is in contrast to the anisotropy observed in simulations of frictionless rough viscoelastic contacts [34].

To demonstrate that the anisotropic changes in macroscopic correlation lengths originate from an anisotropic change in the shape of the individual microjunctions, we extract the time evolution of their equivalent ellipse [the ellipse having the same central second moments as the microjunction; see Fig. 2(c) and the Supplemental Material [30]]. We define their characteristic dimensions $\ell_{\parallel i}$ and $\ell_{\perp i}$ as the lengths of the cords passing through the ellipse center along the directions parallel and orthogonal to shear, respectively (note that, due to the angle θ_i between the major axis of the ellipse and the shear direction, $\ell_{\parallel i}$ and $\ell_{\perp i}$ are different from the major and minor axis lengths of the ellipse). Figure 2(d) shows, for all experiments, the average relative variation in $\ell_{\parallel i}$, $(\ell_{\parallel 0i} - \ell_{\parallel si})/\ell_{\parallel 0i}$, as a function of the average relative variation in $\ell_{\perp i}$, $(\ell_{\perp 0i} - \ell_{\perp si})/\ell_{\perp 0i}$ between the initial state (subscript 0) and that reached when $Q = Q_s$ (subscript s). The positive values of both average relative changes show that, under shear, microjunctions tend to shrink in both directions. The fact that those average points actually lie well above the equality line (by a typical factor of 2 to 3), indicates that most of the microjunctions have a larger change along than orthogonal to the shear direction. Those results are fully consistent with the observed differential changes in $L_\parallel$ and $L_\perp$, indicating that the macroscopic growth of anisotropy essentially originates from a gradual shear-induced shape change of all of the individual microjunctions.

Understanding the shear-induced anisotropy of rough contacts thus amounts to understanding the shape-changing behavior of individual microjunctions. While this shape change is expected to be related to the local tangential force that is applied to a microjunction, the latter force is not a measurable quantity, which impairs direct investigation of the local relationship between aspect ratio and shear force.

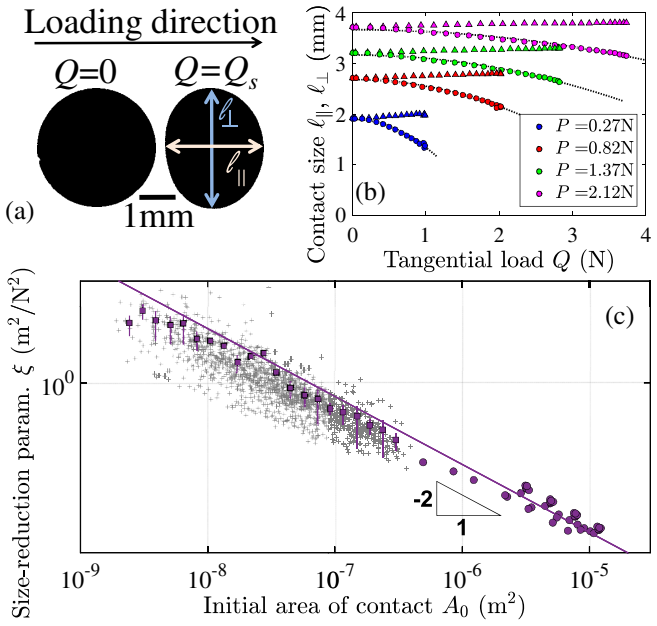

FIG. 3. (a) Segmented images of a smooth sphere-plane contact ($P = 1.10$ N, radius of curvature $R = 9.42$ mm) for $Q = 0$ and Q_s. (Right) Definition of $\ell_\parallel$ and $\ell_\perp$. (b) Evolution of $\ell_\parallel$ (○) and $\ell_\perp$ (△) vs Q, for smooth sphere-plane contacts, for various normal forces. Dotted lines, fits of the form of Eq. (1). (c) Size-reduction parameter ξ vs A_0. Disks, smooth sphere-plane contacts. $R = 7.0$, 9.42, or 24.0 mm. Gray crosses, raw data for microjunctions within multicontacts; squares, average of raw data divided into 21 classes; error bars, standard deviation within each class; solid line, guide for the eye, slope −2.

In order to get some insight on this relationship, we analyze complementary experiments on smooth PDMS-sphere–glass-plane contacts (see Ref. [7] for experimental details). The assumption is that those contacts are good proxies for individual microjunctions, with the advantage that the tangential force applied to them can be accurately measured. Figure 3(a) shows the evolution of the contact morphology of such a smooth sphere-plane contact under shear. The contact initially has a circular shape, which progressively changes as the shear force grows, to an ellipselike shape oriented orthogonal to the shear direction. This is in qualitative agreement with our observations on individual microjunctions.

Figure 3(b) further shows the evolution of the contact sizes along (orthogonal to) the loading direction, $\ell_\parallel$ ($\ell_\perp$), as functions of the tangential force Q. For all normal forces, $\ell_\perp$ shows only small variations, while the larger variations of $\ell_\parallel$ are well captured by an empirical quadratic function of the form (the dotted lines)

$$\ell_\parallel(Q) = \ell_{\parallel 0} - \xi Q^2, \tag{1}$$

with the fitting parameter ξ being *a priori* dependent on all system parameters other than Q. One of the parameters that

we could both change and monitor systematically is the initial area of the contact, A_0. Figure 3(c) (disks) shows the evolution of ξ as a function of A_0 for all experiments on smooth sphere-plane contacts. We find that $\xi(A_0)$ is well captured by a power law $\xi \sim {A_0}^{\delta}$ with $\delta \simeq -2$.

We now come back to rough contacts and assume that each microjunction behaves according to Eq. (1): $\ell_{\parallel i}(q_i) = \ell_{\parallel 0i} - \xi_i q_i^2$, with q_i being the tangential force on microjunction i. Following Ref. [7], we further assume that, at the onset of macroscopic sliding (index s), i.e., when $A_i = A_{si}$, then $q_i = q_{si} = \sigma A_{si}$, with $\sigma = 0.23$ MPa being the frictional shear strength of the rough PDMS-glass interface. We can thus estimate ξ_i as $\xi_i = [(\ell_{\parallel 0i} - \ell_{\parallel si})/(\sigma^2 {A_{si}}^2)]$. In practice, $\ell_{\parallel 0i}$ and $\ell_{\parallel si}$ (A_{0i} and A_{si}) are estimated as the initial and final values of a sigmoid fitted onto the time evolution of ℓ_i (A_i). The resulting values of ξ_i are plotted as a function of A_{0i} as squares in Fig. 3(c). Strikingly, the microjunction data align with the smooth sphere-plane contact data (disks). This suggests a common behavior, for the growth rate of anisotropy under shear, over about 4 orders of magnitude in A_0, from micrometer-scaled microjunctions within multicontacts to millimeter-scaled sphere-plane contacts. We thus expect the same physical origin for the behaviors observed at both ends of the scale range. In this context, understanding the shear-induced anisotropy of smooth sphere-plane contacts appears to be the first step to unravel the anisotropy of sheared rough contacts.

From an empirical standpoint, let us compare the law identified here for the growth of anisotropy of smooth sphere-plane contacts [Eq. (1)] to that found for the concurrent reduction of the contact area, A. In Ref. [7], we found that $A = A_0 - \alpha Q^2$, with $\alpha \sim {A_0}^{\gamma}$ and $\gamma \simeq -3/2$. Both laws are reminiscent of the ones found above for $\ell_{\parallel}$ and ξ, respectively. In order to relate the two sets of observations, we first note that for sphere-plane contacts, $\ell_{\perp}$ remains roughly unchanged under shear, thus suggesting that $\ell_{\perp} \simeq \ell_{\perp 0}$ at all times. Further assuming that the contact takes an elliptic shape, the contact area can thus be written as $A = (\pi/4)\ell_{\parallel}\ell_{\perp} \simeq (\pi/4)\ell_{\parallel}\ell_{\perp 0}$. Replacing A in the area reduction law, dividing by $(\pi/4)\ell_{\perp 0}$, and remembering that $\ell_{\parallel 0} = \ell_{\perp 0} = 2\sqrt{A_0/\pi}$, we obtain $\ell_{\parallel} = \ell_{\parallel 0} - (2\alpha/\sqrt{\pi A_0})Q^2$. The latter expression shows both that (i) the area reduction law and the anisotropy growth law [Eq. (1)] are fully compatible and (ii) $\xi = (2\alpha/\sqrt{\pi A_0})$, thus explaining why the exponents $\delta \simeq -2$ and $\gamma \simeq -3/2$ are found to be related by $\delta = \gamma - 1/2$. In this respect, the present results on shear-induced anisotropy are in good agreement with previous results on contact area reduction under shear in the same systems [7]. They further suggest that the evolution of the area of real contact, A, and thus the value of the static friction force (which is proportional to A), are actually collateral effects of the shear-induced growth of anisotropy described here.

A physics-based model of our experiments on smooth sphere-plane contacts can be found in the companion article [35], which introduces the first fracture-based contact mechanics model accounting for shear-induced anisotropy in adhesive contacts. Once calibrated on one among the present experiments, that model allows us to quantitatively capture the evolution of the contact shape in all other experiments without any more adjustable parameter. In the model of Ref. [35], a vanishing work of adhesion between the contacting surfaces corresponds to an absence of evolution of the contact shape under shear, which suggests that adhesion is likely responsible for the experimentally observed shear-induced anisotropy.

One interesting aspect of the model of Ref. [35] is that it can be used not only on initially circular contacts, like those relevant for the present sphere-plane experiments, but also on initially elliptic contacts with a major axis either parallel or perpendicular to the shear loading direction. The model predicts that when shear is applied along the major axis, the ellipse's eccentricity will tend to decrease, while it will increase when shear is orthogonal to the major axis [35]. Those observations are consistent with the fact that $\ell_{\parallel}$ decreases more than $\ell_{\perp}$ varies under shear. Are those results relevant to rough interfaces, in which microjunctions have a broad distribution of shapes? To test this, we come back to the equivalent ellipse for each microjunction, already used in Fig. 2. We consider all 514 tracked microjunctions with an initial area larger than $2\times10^{-9}\mathrm{m}^2$ in the contact under $P = 6.40$ N. We then calculate Spearman rank correlation coefficient [36] between (i) the set of absolute values of the initial angles, $|\theta_i|$ [Fig. 3(c)], between the shear direction and the major axis of all microjunctions, and (ii) the corresponding set of relative changes in eccentricities between $Q = 0$ and $Q = Q_s$. We find a correlation coefficient of -0.36 with a p value of less than 10^{-16}, which indicates a significant anticorrelation between both quantities. In other words, angles θ_i close to 0° (±90°) statistically correspond to decreasing (increasing) eccentricity under shear, in agreement with the theoretical results.

Overall, our results demonstrate that macroscopic rough elastic contacts can develop significant anisotropy under shear, although the topographies and material properties are isotropic. Such anisotropy develops as soon as shear is applied, well before macroscopic sliding. It originates from a shape change of each microjunction within the interface, presumably due to the existence of adhesive stresses at the interface. Note that, as already discussed in Ref. [7], viscoelasticity is not a likely candidate mechanism because it cannot be responsible for the sustained anisotropy observed in steady sliding, when strains in the elastomer are no longer time dependent. We emphasize that the anisotropy that we describe is essentially reversible, in the sense that separating the two solids and performing again a shear experiment will lead to the exact same behavior.

This is in strong contrast to the persistent contact anisotropy induced either by wear (e.g., asymmetric scars left in the contact zone [37]) or by shear-driven structural changes in the materials (e.g., in fault rocks [38] and in metals [39]), which would act as anisotropy sources in a subsequent sheared contact. Our results pave the way for possible control of the many physical properties affected by contact anisotropy (see the introduction) through application of controlled shear forces on the interface.

This work was supported by LABEX MANUTECH-SISE (ANR-10-LABX-0075) of the Université de Lyon, within the program Investissements d'Avenir (ANR-11-IDEX-0007) operated by the French National Research Agency (ANR). It received funding from the People Program (Marie Curie Actions) of the European Union's Seventh Framework Program (FP7/2007-2013) under Research Executive Agency Grant Agreement No. PCIG-GA-2011-303871. We are indebted to Institut Carnot Ingénierie@Lyon for support and funding. A. P. is thankful to the DFG (German Research Foundation) for funding Project No. PA 3303/1-1. M. C. is supported by the Italian Ministry of Education, University and Research (MIUR) under the "Departments of Excellence" grant L.232/2016.

*Corresponding author.
julien.scheibert@ec-lyon.fr

[1] J. A. Greenwood and J. B. P. Williamson, Contact of nominally flat surfaces, Proc. R. Soc. A **295**, 300 (1966).
[2] B. N. J. Persson, Theory of rubber friction and contact mechanics, J. Chem. Phys. **115**, 3840 (2001).
[3] J. F. Archard, Elastic deformation and the laws of friction, Proc. R. Soc. A **243**, 190 (1957).
[4] J. H. Dieterich and B. D. Kilgore, Direct observation of frictional contacts: New insights for state-dependent properties, Pure Appl. Geophys. **143**, 283 (1994).
[5] F. Wu-Bavouzet, J. Cayer-Barrioz, A. Le Bot, F. Brochard-Wyart, and A. Buguin, Effect of surface pattern on the adhesive friction of elastomers, Phys. Rev. E **82**, 031806 (2010).
[6] E. Degrandi-Contraires, C. Poulard, F. Restagno, and L. Léger, Sliding friction at soft micropatterned elastomer interfaces, Faraday Discuss. **156**, 255 (2012).
[7] R. Sahli, G. Pallares, C. Ducottet, I. E. Ben Ali, S. Al Akhrass, M. Guibert, and J. Scheibert, Evolution of real contact area under shear and the value of static friction of soft materials, Proc. Natl. Acad. Sci. U.S.A. **115**, 471 (2018).
[8] B. Weber, T. Suhina, T. Junge, L. Pastewka, A. Brouwer, and D. Bonn, Molecular probes reveal deviations from Amontons' law in multi-asperity frictional contacts, Nat. Commun. **9**, 888 (2018).
[9] J. A. Greenwood, Br., Constriction resistance and the real area of contact, J. Appl. Phys. **17**, 1621 (1966).
[10] V. L. Popov, *Contact Mechanics and Friction* (Springer, Berlin, 2017).
[11] S. Medina, D. Nowell, and D. Dini, Analytical and numerical models for tangential stiffness of rough elastic contacts, Tribol. Lett. **49**, 103 (2013).
[12] R. Aghababaei, D. H. Warner, and J.-F. Molinari, On the debris-level origins of adhesive wear, Proc. Natl. Acad. Sci. U.S.A. **114**, 7935 (2017).
[13] M. Scaraggi and B. N. J. Persson, Friction and universal contact area law for randomly rough viscoelastic contacts, J. Phys. Condens. Matter **27**, 105102 (2015).
[14] J. H. Dieterich and B. D. Kilgore, Imaging surface contacts: power law contact distributions and contact stresses in quartz, calcite, glass and acrylic plastic, Tectonophysics **256**, 219 (1996).
[15] G. Carbone and C. Putignano, Rough viscoelastic sliding contact: Theory and experiments, Phys. Rev. E **89**, 032408 (2014).
[16] L. Pastewka and M. O. Robbins, Contact between rough surfaces and a criterion for macroscopic adhesion, Proc. Natl. Acad. Sci. U.S.A. **111**, 3298 (2014).
[17] A. W. Bush, R. D. Gibson, and T. R. Thomas, The elastic contact of a rough surface, Wear **35**, 87 (1975).
[18] V. A. Yastrebov, G. Anciaux, and J.-F. Molinari, The role of the roughness spectral breadth in elastic contact of rough surfaces, J. Mech. Phys. Solids **107**, 469 (2017).
[19] A. I. Vakis *et al.*, Modeling and simulation in tribology across scales: An overview, Tribol. Int. **125**, 169 (2018).
[20] G. Carbone, B. Lorenz, B. N. J. Persson, and A. Wohlers, Contact mechanics and rubber friction for randomly rough surfaces with anisotropic statistical properties, Eur. Phys. J. E **29**, 275 (2009).
[21] K. L. Johnson, *Contact Mechanics* (Cambridge University Press, Cambridge, England, 1987).
[22] J. Barber and M. Ciavarella, JKR solution for an anisotropic half space, J. Mech. Phys. Solids **64**, 367 (2014).
[23] K. E. Koumi, T. Chaise, and D. Nelias, Rolling contact of a rigid sphere/sliding of a spherical indenter upon a viscoelastic half-space containing an ellipsoidal inhomogeneity, J. Mech. Phys. Solids **80**, 1 (2015).
[24] C. Frétigny and A. Chateauminois, Contact of a spherical probe with a stretched rubber substrate, Phys. Rev. E **96**, 013001 (2017).
[25] A. R. Savkoor and G. A. D. Briggs, The effect of tangential force on the contact of elastic solids in adhesion, Proc. R. Soc. A **356**, 103 (1977).
[26] M. Varenberg and S. Gorb, Shearing of fibrillar adhesive microstructure: friction and shear-related changes in pull-off force, J. R. Soc. Interface **4**, 721 (2007).
[27] G. Petitet and M. Barquins, *Matériaux Caoutchouteux: Morphologies, Formulations, Adhérence, Glissance et Usure* (Presses polytechniques et universitaires romandes, Lausanne, Switzerland, 2008).
[28] J. F. Waters and P. R. Guduru, Mode-mixity-dependent adhesive contact of a sphere on a plane surface, Proc. R. Soc. A **466**, 1303 (2010).
[29] J. C. Mergel, R. Sahli, J. Scheibert, and R. A. Sauer, Continuum contact models for coupled adhesion and friction, J. Adhes., https://doi.org/10.1080/00218464.2018.1479258 (2018).
[30] See Supplemental Material at http://link.aps.org/supplemental/10.1103/PhysRevLett.122.214301, which includes Refs. [31–33], for a typical power spectral density of

the topographies used, for details of the image analysis procedure, and for a typical exponential fit of the autocorrelation function of the segmented images.

[31] T. D. B. Jacobs, T. Junge, and L. Pastewka, Quantitative characterization of surface topography using spectral analysis, Surf. Topogr.: Metrol. Prop. **5**, 013001 (2017).

[32] F. Lechenault, G. Pallares, M. George, C. Rountree, E. Bouchaud, and M. Ciccotti, Effects of Finite Probe Size on Self-Affine Roughness Measurements, Phys. Rev. Lett. **104**, 025502 (2010).

[33] N. Ponthus, J. Scheibert, K. Thøgersen, A. Malthe-Sørenssen, and J. Perret-Liaudet, Statistics of the separation between sliding rigid rough surfaces: Simulations and extreme value theory approach, Phys. Rev. E **99**, 023004 (2019).

[34] C. Putignano and G. Carbone, Viscoelastic reciprocating contacts in presence of finite rough interfaces: A numerical investigation, J. Mech. Phys. Solids **114**, 185 (2018).

[35] A. Papangelo, J. Scheibert, R. Sahli, G. Pallares, and M. Ciavarella, Shear-induced contact area anisotropy explained by a fracture mechanics model, Phys. Rev. E **99** 053005 (2019).

[36] C. Spearman, The proof and measurement of association between two things, Am. J. Psychol. **15**, 72 (1904).

[37] A. Tiwari, L. Dorogin, B. Steenwyk, A. Warhadpande, M. Motamedi, G. Fortunato, V. Ciaravola, and B. N. J. Persson, Rubber friction directional asymmetry, Europhys. Lett. **116**, 66002 (2016).

[38] C. Collettini, A. Niemeijer, C. Viti, and C. Marone, Fault zone fabric and fault weakness, Nature (London) **462**, 907 (2009).

[39] S. Deng, A. Godfrey, W. Liu, and C. Zhang, Microstructural evolution of pure copper subjected to friction sliding deformation at room temperature, Mater. Sci. Eng. A **639**, 448 (2015).